Doctorate of Philosophy

Schrödinger's Catwalk

Brian Flynn

University of Bristol

November, 2020

CONTENTS

ACRONYMS

BF Bayes factor. 2, 11

EDH experiment design heuristic. 7, 8
ES exploration strategy. 2, 11, 16

FH Fermi-Hubbard. 9

QHL quantum Hamiltonian learning. 5, 7, 8, 16
QMLA Quantum Model Learning Agent. i, 2, 3, 11, 16

GLOSSARY

Jordan Wigner transformation (JWT) Jordan Wigner transformation . 10

instance a single implementation of the Quantum Model Learning Agent (QMLA) algorithm. 16

probe Input probe state, $|\psi\rangle$, which the target system is initialised to, before unitary evolution. plural. 5

run collection of QMLA instances. 16

volume Volume of a parameter distribution's credible region.. 6–8

Part I

THEORETICAL STUDY

1

PRESCRIBED MODEL SETS

A sensible first case study for the QMLA framework is to prescribe a set of models, where we know that the true model is among them, or at least that we would be satisfied with approximating $\hat{H}_0$ as the best model in the set. This application can be useful, for example, for expedited device calibration; suppose we wish to characterise a new, untrustued quantum simulator/device, S_u, and we have access to a *trusted*[1] simulator, S_t. In order to perform this calibration, we treat S_u as the system, Q, i.e. we call upon it to retrieve the datum d in **??**, where the calculation of the likelihoods for each particle are computed through S_t. If S_u is reliable, the data from its calculations will be consistent with some $\hat{H}_0$ of our choosing, while miscalibrations will mainfest as imperfectly implemented gates/steps in the calculation of the system's likelihood, and so would result in data inconsistent with $\hat{H}_0$. Therefore, if we can prescribe the most likely miscalibrations, it may be feasible to compose a set of models, $\mathbb{H}$, which represent those cases, and search for $\hat{H}'$ only within $\mathbb{H}$, to find idenfitfy the miscalibrations. For example, by encoding connections between every pair of device qubits in $\hat{H}_0$, we can compose models with restricted connectivity, for instance where some pairs of qubits are disconnected, and hence discover whether the device allows arbitrary two-qubit gates, and which pairs are disallowed.

1.1 LATTICES

We first consider Q as some lattice, where QMLA attempts to identify the structure of the lattice. The set of viable models then comprises alternative lattices. Due to simluation constraints, because we train models through exact unitary evolution, we are restricted to $\sim$ 8-qubit Hamiltonians, so we only consider lattices which can be simulated in this limit. The exploration strategy (ES) in this chapter is then simply to propose a set of models with no further model generation, with comparisons between all pairs of models through Bayes factors (BFs).

Connectivity between lattice sites is achieved within the specific Hamiltonian formalisms introduced in the following sections, although in general we write $\mathcal{C} = \{\langle k, l\rangle\}$ as the set of connected pairs $\langle k, l\rangle$, such that the Hamiltonian for a given lattice can be thought of as some function of its configuration, $\hat{H}(\vec{\alpha}, \mathcal{C})$. Then, we can specify candidate models only by their $\mathcal{C}$, e.g. a 3-site chain can be summarised by $\mathcal{C} = \{\langle 1,2\rangle, \langle 2,3\rangle\}$, whereas a fully connected 3-site lattice (i.e. a triangle) is given by $\mathcal{C} = \{\langle 1,2\rangle, \langle 1,3\rangle, \langle 2,3\rangle\}$. We can then summarise the set of candidate models through the descriptions of lattice configurations, corresponding to those depicted in Fig. 1.1:
a. 2-site chain

1 Note: here a classical computer can fulfil the role of the trusted simulator.

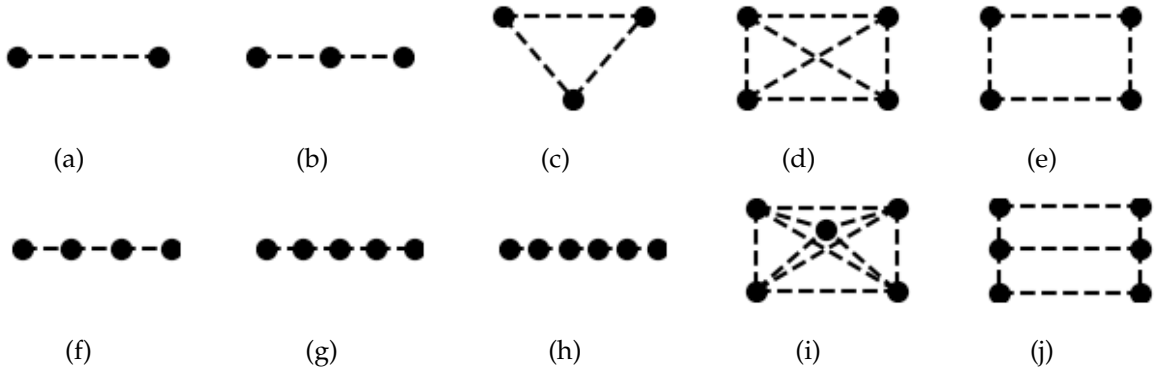

Figure 1.1: Lattices used for prescribed models test for QMLA. Lattices are characterised by the connectivity of their sites; dotted lines show connection between pairs of sites.

b. 3-site chain
c. 3-site fully connected (triangle)
d. 4-site fully conneted (square)
e. 4-site linearly connected (loop)
f. 4-site chain
g. 5-site chain
h. 6-site chain
i. 5-site fully connected (pentagon)
j. 6-site partially connected (grid)

We will use this set of lattice configurations throughout the remainder of this chapter.

1.2 ISING MODEL

The Ising model is one of the most studied concepts in all of physics, representing electrons on a lattice of N sites, where each electron can have *spin* up or down. Interactions between spins $\langle k, l \rangle$ have strength J_{kl}, and the transverse magnetic field acting uniformly on all sites with strength h. It is usually stated as

$$\hat{H}_I(\mathcal{C}) = -\sum_{\langle k,l \rangle \in \mathcal{C}} J_{kl}\, \hat{\sigma}_k^z\, \hat{\sigma}_l^z + h \sum_{k=1}^{N} \hat{\sigma}_k^x. \tag{1.1}$$

The interacion term indicates the class of magnetism of the pair's interaction, i.e.

$$\begin{cases} J_{kl} > 0, & \text{ferromagnetic} \\ J_{kl} < 0, & \text{antiferromagnetic} \\ J_{kl} = 0, & \text{noninteracting.} \end{cases} \tag{1.2}$$

If all interaction pairs are described by the same case in Eq. (1.2), the entire system can be said belong to that class of magnetism.

1.2.1 *Note on optimising the Ising model*

Many treatments of the Ising model seek to find the ground state of the system by optimising the configuration of spins in the system. This involves neglecting the transverse magnetic field, and treating Ising model classically, such that the ground state is found by minimising the energy function

$$E_I = \langle\psi|H_I|\psi\rangle = \sum_{\langle k,l\rangle\in\mathcal{C}} J_{kl}\ \langle\psi|\hat{\sigma}_k^z\,\hat{\sigma}_l^z|\psi\rangle\,, \tag{1.3}$$

where $|\psi\rangle = |\psi_1\rangle \otimes |\psi_2\rangle \cdots \otimes |\psi_N\rangle$.

This optimisation relies on the relationship between the Ising model with its eigenvalues and eigenstates: Eq. (1.3) consists only of $\hat{\sigma}^z$ terms, and we have that

$$\hat{\sigma}^z\,|+\rangle = +1\,|+\rangle \quad ; \quad \hat{\sigma}^z\,|-\rangle = -1\,|-\rangle\,. \tag{1.4}$$

Then, for a single pair of spins $\langle k,l\rangle$, we have

$$\begin{aligned}
\langle +_k\,+_l|\,\hat{\sigma}_k^z\,\hat{\sigma}_l^z\,|+_k\,+_l\rangle &= \langle +_k\,+_l|\,(+1)(+1)\,|+_k\,+_l\rangle = +1,\\
\langle +_k\,-_l|\,\hat{\sigma}_k^z\,\hat{\sigma}_l^z\,|+_k\,-_l\rangle &= \langle +_k\,-_l|\,(+1)(-1)\,|+_k\,-_l\rangle = -1,\\
\langle -_k\,+_l|\,\hat{\sigma}_k^z\,\hat{\sigma}_l^z\,|-_k\,+_l\rangle &= \langle -_k\,+_l|\,(-1)(+1)\,|-_k\,+_l\rangle = -1,\\
\langle -_k\,-_l|\,\hat{\sigma}_k^z\,\hat{\sigma}_l^z\,|-_k\,-_l\rangle &= \langle -_k\,+_l|\,(-1)(1)\,|-_k\,-_l\rangle = +1.
\end{aligned} \tag{1.5}$$

So, by restricting the individual spins to $|\psi_k\rangle \in \{|+\rangle\,, |-\rangle\}$, we can equivalently consider every spin s_k in the system as a binary variable $s_k \in \{\pm 1\}$, i.e. $s_k s_l = \pm 1$ in Eq. (1.5), such that the energy function

$$E_I(\mathcal{S}) = \langle\psi|\hat{H}_I|\psi\rangle = \sum_{\langle k,l\rangle\in\mathcal{C}} J_{kl}\ \ s_k s_l \tag{1.6}$$

can be minimised by optimising the configuration $\mathcal{S}$. The optimal configuration $\mathcal{S}_0$ can then be mapped to a state vector $|\psi_0\rangle$, i.e. the ground state of the system.

While this task can be greatly simplified by the reduction in Eq. (1.5), meaning we do not have to compute any unitary evolution to evaluate Eq. (1.6), it is still an expensive optimisation, because effectively it is a search over $\{|\psi\rangle\}$, so the search space has 2^N candidates [1, 2]. This allows for a straightforward mapping between ground state search and solving combinatorial optimsiation algorithms, namely MAX-CUT, known to be NP-complete [3]. This mapping underlies ongoing research into quantum annealing as a computational platform capable of providing advantage for a specific family of problems [4, 5, 6].

Crucially, our goal is *not* to find the ground state of Q, but instead to find the generator of its dynamics for the system. Therefore, we treat the Ising *quantum mechanically*: instead of treating

	$J_{\langle k,l\rangle}$	h_k
Standard	J	h
Fully parameterised	$J_{\langle k,l\rangle}$	h_k

Table 1.1: Types of Ising model.

Eq. (1.1) as the underlying mechanism for a cost function to be optimised, i.e. Eq. (1.6), we use quantum operators and do not necessarily restrict the probe state $|\psi\rangle$, allowing us to use Eq. (1.1) within the likelihood function **??**.

1.2.2 *Ising model cases*

We consider two cases: firstly, where it is assumed that the strength of interactions $J_{k,l}$ are uniform (given by J); and secondly, where each interaction is assigned a unique parameter (J_{kl}). In the first case, can represent the Ising model for a given lattice configuration $\mathcal{C}$ as

$$\hat{H}(\mathcal{C}) = J \sum_{\langle k,l\rangle \in \mathcal{C}} \hat{\sigma}_k^z \hat{\sigma}_l^z + h \sum_{k=1}^{N} \hat{\sigma}_k^x, \tag{1.7}$$

allowing for the compact representation, following **??**,

$$\vec{\alpha}_I = \begin{pmatrix} J & h \end{pmatrix} \tag{1.8a}$$

$$\vec{T}_I = \begin{pmatrix} \sum\limits_{\langle k,l\rangle \in \mathcal{C}} \hat{\sigma}_k^z \hat{\sigma}_l^z \\ \sum\limits_{k=1}^{N} \hat{\sigma}_k^x \end{pmatrix}. \tag{1.8b}$$

In the more general second case, termed the *fully parameterised* Ising model, we instead have the term set

$$\mathcal{T}_I = \left\{ \hat{\sigma}_k^z \hat{\sigma}_l^z, \ \sum_{k=1}^{N} \hat{\sigma}_k^x \right\}_{\langle k,l\rangle \in \mathcal{C}}. \tag{1.9}$$

with unique parameters J_{kl} associated with each interaction term $\hat{\sigma}_k^z \hat{\sigma}_l^z$. We summarise theses cases in Table 1.1

We can first construct models under each of these forms to verify quantum Hamiltonian learning (QHL) is applicable. The former case is the form standard of the Ising model; its training is shown in Fig. 1.2, while the fully paramterised model is shown in Fig. 1.3. In this case, the fully parameterised model will learn the same parameters as the standard Ising model, i.e. $J_k^z = J^z; J_k^x = J^x$. Unsurprisingly, the two-parameter model learns its parameters faster,

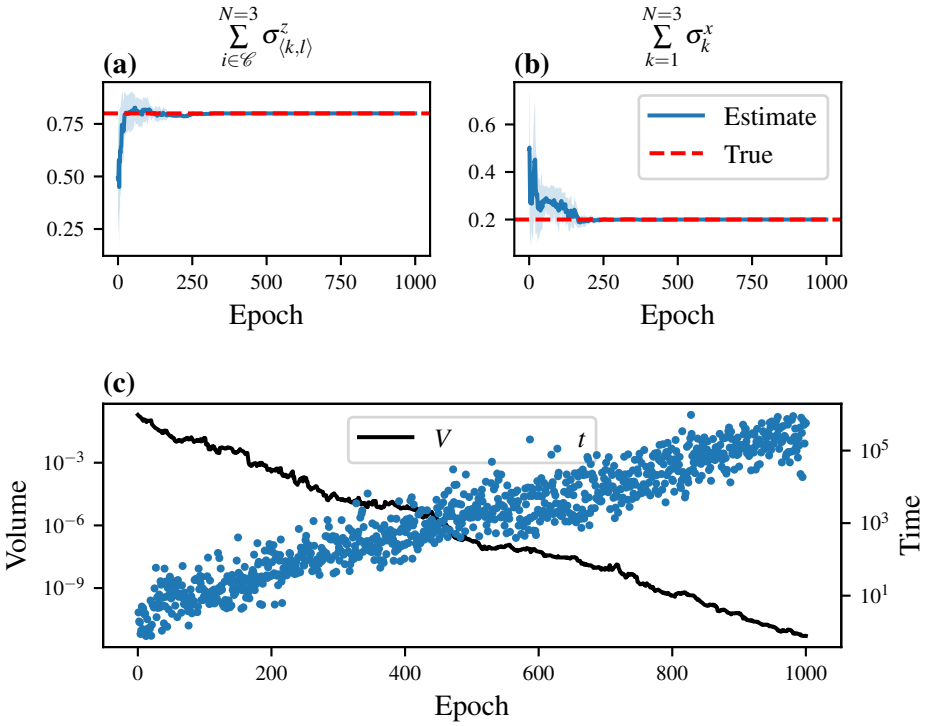

Figure 1.2: QHL for Ising model where terms are grouped by their functionality, as in Eq. (1.1). (a,b) show the parameter estimates progression against epochs (experiments), with the corresponding term written on top of the plot; (c) shows the volume of the parameter distribution at each epoch, as well as the evolution time chosen by the experiment design heuristic (EDH). Implementation details are listed in Table A.1

whereas the fully parameterised model required double the number of experiments to learn the parameters well. Interestingly, neither model converged; the volume continues to reduce exponentially in both cases, suggesting it may be impractical to seek saturation in the model training phase for every model, since this may require a very large number of experiments and particles.

The dynamics produced by both models are shown in Fig. 1.4: the dynamics are almost indistinguishable by eye, but the standard Ising model, which in this case is $\hat{H}_0$, outperforms the fully parameterised model, by a BF of 10^{19}. This serves as a good *sanity check*, confirming our expectation that the BF will favour the simpler model (i.e. fewer parameters) even when both models are trained to a high precision, and are difficult to distinguish through human intuition.

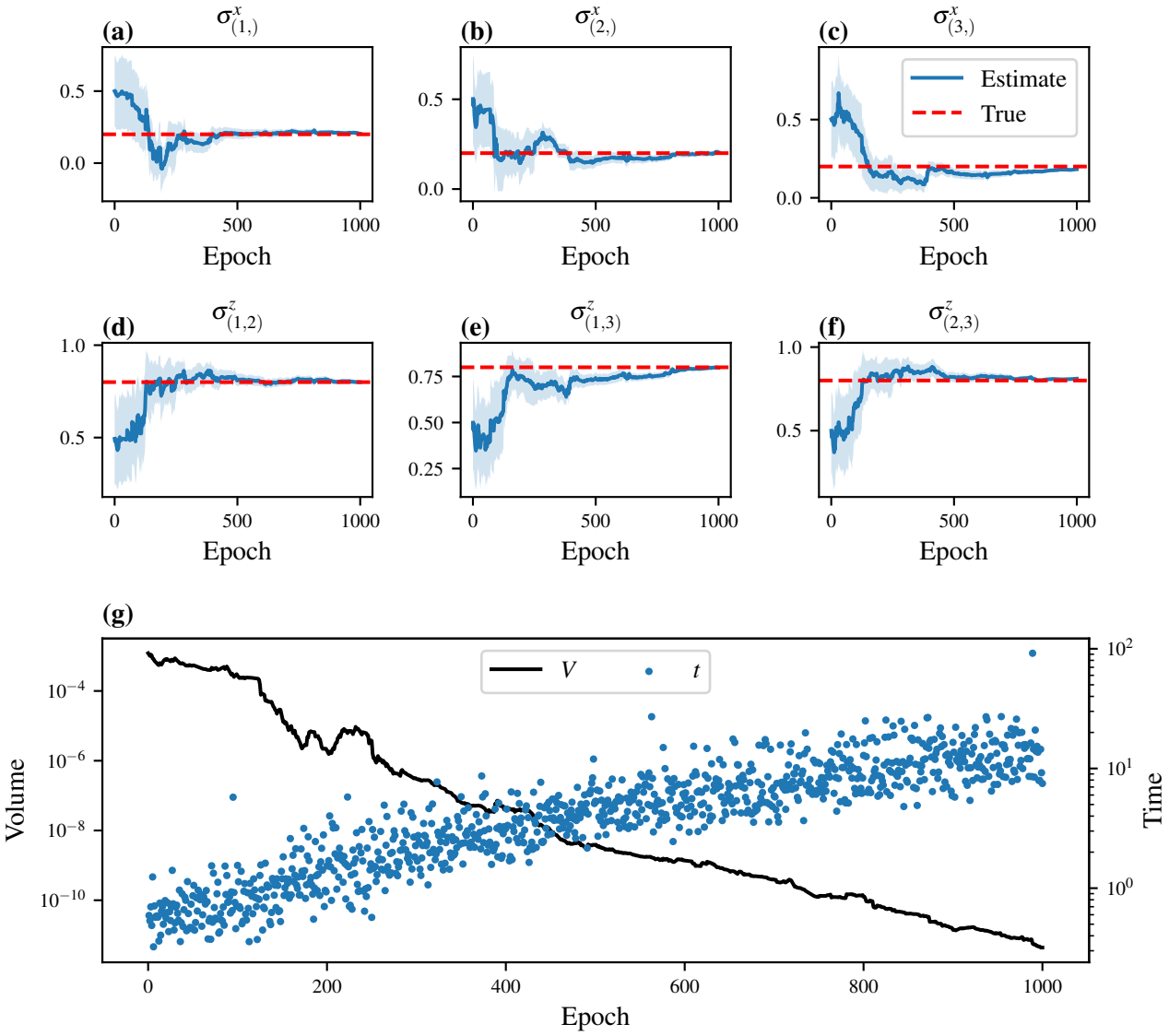

Figure 1.3: QHL for fully parameterised Ising model, where every interaction between pairs of sites are assigned unique parameters, here neglecting the transverse field, as in Eq. (1.9). (a)-(f) show the parameter estimates progression against epochs (experiments), with the corresponding term written on top of the plot; (g) shows the volume of the parameter distribution at each epoch, as well as the evolution time chosen by the EDH. Implementation details are listed in Table A.1

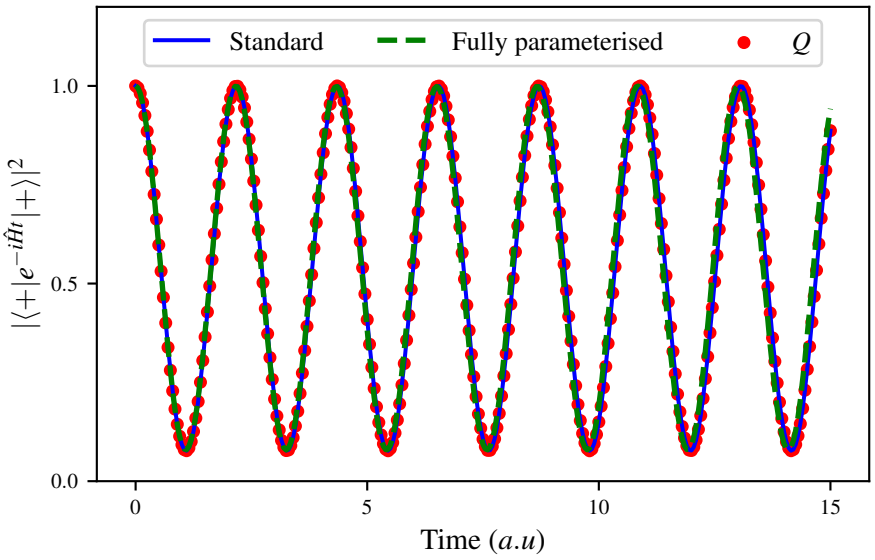

Figure 1.4: Dynamics reproduced by Ising models under standard and fully parameterised formalisms, compared with dynamics for the true system.

1.3 HEISENBERG MODEL

Generalising the Ising model, the Heisenberg Hamiltonian is another model for magnetic systems consisting of a set of spins on a lattice [7]. It builds on the Ising model by additionally considering the spins' rotations about the $x-$ and $y-$ axes, generally stated as

$$\hat{H}_H(\mathcal{C}) = \sum_{\langle k,l\rangle\in\mathcal{C}} J^x_{kl}\ \hat{\sigma}^x_k\hat{\sigma}^x_l + \sum_{\langle k,l\rangle\in\mathcal{C}} J^y_{kl}\ \hat{\sigma}^y_k\hat{\sigma}^y_l + \sum_{\langle k,l\rangle\in\mathcal{C}} J^z_{kl}\ \hat{\sigma}^z_k\hat{\sigma}^z_l + \sum_{k=1}^{N} h_k\hat{\sigma}^z_k. \tag{1.10}$$

We can consider a number of formulations of the Heisenberg model, by considering whether the interaction parameters are completely unique for each pair of spins in each axis, or are shared by pairs of spins; we list the instances within the family of Heisenberg models in Table 1.2.

Again, there are a number of possibile models to test, although we can reasonably expect these to follow the same arguments as for the Ising model cases: increasing generality at the expense of larger parameter dimension requires more resources to learn to a reasonable level. In this chapter we will refer to the Heisenberg-XYZ model, and will consider the fully parameterised Heisenberg model in Chapter 3.

$$\vec{\alpha}_H = (J^x \quad J^y \quad J^z \quad h) \tag{1.11a}$$

	J^x_{kl}	J^y_{kl}	J^z_{kl}	h_k
XXX	J^x	J^x	J^x	h
XXZ	J^x	J^x	J^z	h
XYZ (standard)	J^x	J^y	J^z	h
Fully parameterised	J^x_{kl}	J^y_{kl}	J^z_{kl}	h_k

Table 1.2: Heisenberg model types: varying whether the interaction parameters J^w_{kl} are shared among pairs of spins give distinct descriptions which are all in the family of Heisenberg models.

$$\vec{T}_H = \begin{pmatrix} \sum_{\langle k,l\rangle\in\mathcal{C}} \hat{\sigma}^x_k \hat{\sigma}^x_l \\ \sum_{\langle k,l\rangle\in\mathcal{C}} \hat{\sigma}^y_k \hat{\sigma}^y_l \\ \sum_{\langle k,l\rangle\in\mathcal{C}} \hat{\sigma}^z_k \hat{\sigma}^z_l \\ \sum_{k=1}^{N} \hat{\sigma}^z_k \end{pmatrix} \tag{1.11b}$$

1.4 HUBBARD MODEL

Another representation of solid state matter systems is given by the Hubbard model [8, 9, 10]. The Hubbard model deals with systems of correlated fermions, allowing spins to *hop* between sites. Note the Hubbard model is synonymous with the Fermi-Hubbard (FH) model, which can be used to distinguish this model of fermions from a similar model of bosons, captured by the Bose-Hubbard model, which is not studied in this thesis. We use the subscript FH to distinguish the (Fermi-)Hubbard model from the Heisenberg model $\hat{H}_H$, Eq. (1.10). The Hubbard model is generally stated in second quantisation as

$$\hat{H}_{FH}(\mathcal{C}) = \sum_{s\in\{\uparrow,\downarrow\}} \sum_{\langle k,l\rangle\in\mathcal{C}} t^s_{\langle k,l\rangle} \left(\hat{c}^\dagger_{ks} c_{ls} + \hat{c}^\dagger_{ls} c_{ks}\right) + \sum_k^N U_k \hat{n}_{k\uparrow}\hat{n}_{k\downarrow} + \sum_k^N \mu_k \left(\hat{n}_{k\uparrow} + \hat{n}_{k\downarrow}\right) \tag{1.12}$$

where

- $\hat{c}_{ks}$ and $\hat{c}^\dagger_{ks}$ are respecitvely the fermionic annihilation and creation operators for spin $s \in \{\uparrow,\downarrow\}$ on site k;
- $\hat{n}_{ks} = \hat{c}^\dagger_{ks}\hat{c}_{ks}$ is a counting operator to count the number of spins s on site k;
- $t^s_{\langle k,l\rangle}$ is the kinetic (hopping) term for spin s between sites k and l;
- U_k is the onsite (repulsion) energy for site k;

	$t^{\uparrow}_{\langle k,l\rangle}$	$t^{\uparrow}_{\langle k,l\rangle}$	U_k	μ_k
Standard	$t^{\uparrow}$	$t^{\downarrow}$	U	μ
Fully parameterised	$t^{\uparrow}_{\langle k,l\rangle}$	$t^{\downarrow}_{\langle k,l\rangle}$	U_k	μ_k

Table 1.3: Types of Hubbard model.

- μ_k is the chemical energy for k;
- N is the number of sites in the system.

Again, we can achieve differing physics through controlling whether the parameters are shared, with similar consequences to the Ising and Heisenberg models, where additional parameterisation comes at the expense of slower/worse performance in training. We list a subset of possible configurations in Table 1.3; we will use the standard form in this chapter, i.e.

$$\vec{\alpha}_{FH} = (t^{\uparrow} \quad t^{\downarrow} \quad U \quad \mu) \tag{1.13a}$$

$$\vec{T}_{FH} = \begin{pmatrix} \sum_{\langle k,l\rangle\in\mathcal{C}} (\hat{c}^{\dagger}_{k,\uparrow}\hat{c}_{l,\uparrow} + \hat{c}^{\dagger}_{l,\uparrow}\hat{c}_{k,\uparrow}) \\ \sum_{\langle k,l\rangle\in\mathcal{C}} (\hat{c}^{\dagger}_{k,\downarrow}\hat{c}_{l,\downarrow} + \hat{c}^{\dagger}_{l,\downarrow}\hat{c}_{k,\downarrow}) \\ \sum_{k=1}^{N} \hat{n}_{k\uparrow}\hat{n}_{k\downarrow} \\ \sum_{k=1}^{N} (\hat{n}_{k\uparrow} + \hat{n}_{k\downarrow}) \end{pmatrix} \tag{1.13b}$$

1.4.1 *Jordan Wigner transformation*

In order that the Hubbard model is simulateable with qubits[2], it must first undergo a mapping from the fermionic representation to a spin system representation; such a mapping is given by the Jordan Wigner transformation (JWT) [11, 12].

In second quantisation, the fermions on the lattice can occupy one (or a superposition of) *modes*, for example, spin ↑ on the site indexed 3 is a mode. The system can then be given by a state in the *number basis*,

$$|\psi_f\rangle = |n_{m_1}, n_{m_2}, \ldots, n_{m_n}\rangle\,, \tag{1.14}$$

where n_{m_i} is the number of fermions on mode m_i and there are n modes in total.

$\hat{c}^{\dagger}_{m_i}$ ($\hat{c}_{m_i}$) is the creation (annihilation) operator on the mode m_i: it acts on the system by adding (removing) a fermion from (to) m_i:

$$\hat{c}^{\dagger}_{m_i}|\psi_f\rangle = |n_{k_1}, \ldots, n_{m_i}+1, \ldots, n_{k_n}\rangle\,, \tag{1.15a}$$

2 Or simulations of qubits, as in this thesis.

Mode	Site	Spin	Qubit
1	1	↑	1
2	1	↓	2
3	2	↑	3
4	2	↓	4
	⋮		
$2N-1$	N	↓	$2N-1$
$2N$	N	↑	$2N$

Table 1.4: Jordan Wigner mode/qubit indices.

$$\hat{c}_{m_i} |\psi_f\rangle = |n_{k_1}, \ldots, n_{m_i} - 1, \ldots, n_{k_n}\rangle . \tag{1.15b}$$

In the Hubbard model, we assign a mode for each combination of spin $s \in \{\uparrow, \downarrow\}$ with each site k, i.e. the system is in the state

$$|\psi_{FH}\rangle = |n_{1\uparrow}, n_{1\downarrow}, \ldots, n_{N\uparrow}, n_{N\downarrow}\rangle . \tag{1.16}$$

In particular, since fermions obey the Pauli exclusion principle, we have $n_{sk} \in \{0, 1\} \forall s, k$, i.e. every spin/site can be occupied by at most one electron, and we can view them as two-level systems. Then, to map the number basis of Eq. (1.16) to a state which cab be prepared on qubits, the JWT assigns a single qubit to each mode, where qubits are ordered simply by the site index and spin type, as shown in Table 1.4. The JWT can be summarised by mapping – for the mode m – the creation (annihilation) operator $\hat{c}_m^\dagger$ ($\hat{c}_m$), to an operator which adds a spin to the corresponding state through the operator $\hat{\sigma}_m^+$ ($\hat{\sigma}_m^-$).

$$\hat{c}_m \to (\hat{\sigma}^z)^{\otimes k-1} \otimes \hat{\sigma}^- \otimes (\hat{\sigma}^z)^{\otimes 2N-1} \tag{1.17a}$$

$$\hat{c}_m^\dagger \to (\hat{\sigma}^z)^{\otimes k-1} \otimes \hat{\sigma}^+ \otimes (\hat{\sigma}^z)^{\otimes 2N-1} \tag{1.17b}$$

Empty lattices are thus given by $|0\rangle^{\otimes 2N}$. For example, an empty 2-site lattice $|\psi_0\rangle$ is acted on by a creation operator on mode 3, corresponding to spin ↑ on site 2:

$$\hat{c}_{2\uparrow}^\dagger |0000\rangle = \hat{c}_3^\dagger |0000\rangle = \hat{\sigma}_1^z \hat{\sigma}_2^z \hat{\sigma}_3^+ \hat{\sigma}_4^z |0000\rangle = |0010\rangle \tag{1.18}$$

1.4.2 *Half filled basis*

In principle there can be $2N$ spins on a lattice of N sites, although in general we will restrict to the case where there are N spins in the lattice, known as *half-filling*, such that Eq. (1.16) is

effectively projected into the subspace spanned by half-filled basis states. For example, with $N = 2$

$$\{|1100\rangle, |1010\rangle, |1001\rangle, |0101\rangle, |0110\rangle, |0011\rangle\} \tag{1.19}$$

Therefore, in the design of probes for training Hubbard models, we can generate probes in the subspace spanned by half-filled states.

1.5 MODEL LEARNING FOR LATTICES

Finally, then, we can use the lattice systems introduced in Sections 1.1 to 1.4 as firsts case studies for QMLA. Each $\mathcal{C} \in \mathbb{C}$ can specify a unique model under the standard model formalism for each of Ising (Eq. (1.8)), Heisenberg (Eq. (1.11)) and Hubbard (Eq. (1.13)) models. We can then devise a simple ES which only tests the models corresponding to $\mathbb{C}$, with no further model generation, i.e. Algorithm 1, and compares every pair of models through BF, deeming the champion as that which wins the largest number of comparisons, as in Algorithm 2.

Algorithm 1: Lattice exploration strategy: model generation

Input: $\mathbb{C}$ // Set of lattice configurations
Output: $\{\hat{H}_i\}$ // Set of models to tests

$\mathbb{H} = \{\ \}$
for $\mathcal{C} \in \mathbb{C}$ **do**
  $\hat{H}_i \leftarrow \text{map\_lattice\_to\_model}(\mathcal{C})$
  $\mathbb{H} \leftarrow \mathbb{H} \cup \{\hat{H}_i\}$
end
return $\mathbb{H}$

For example, we adopt the fully connected four site lattice (d in Fig. 1.1) as the true lattice specifying $\hat{H}_0$, under the Ising formalism (Eq. (1.7)) in Fig. 1.5. We can then run QMLA by training each model (Fig. 1.5a-b); comparing the models predictive power (Fig. 1.5c-d) through BF (Fig. 1.5e), and choosing the model which wins the largest number of BF contests. In this example, $\hat{H}_0$ is stronger than every alternative model according to the BFs, and is hence determined as $\hat{H}'$.

In order to test QMLA robustly, we can use each of the lattices shown in Fig. 1.1 to specify $\hat{H}_0$, to ensure the algorithm is capable of finding the underlying model of arbitrary complexity, within the constraints of a prescribed model set[3]. Moreover, we can extend this test to the Heisenberg and Hubbard formalisms; note that due to the overhead given by the JWT (Section 1.4.1), i.e. the requirement of two qubits per site, we restrict study of the Hubbard model to lattices $a - e$ for practicality. By running 10 independent QMLA instances for each lattice under each formalism we can gauge the success rate of the algorithm for distinguishing basic lattices from each other.

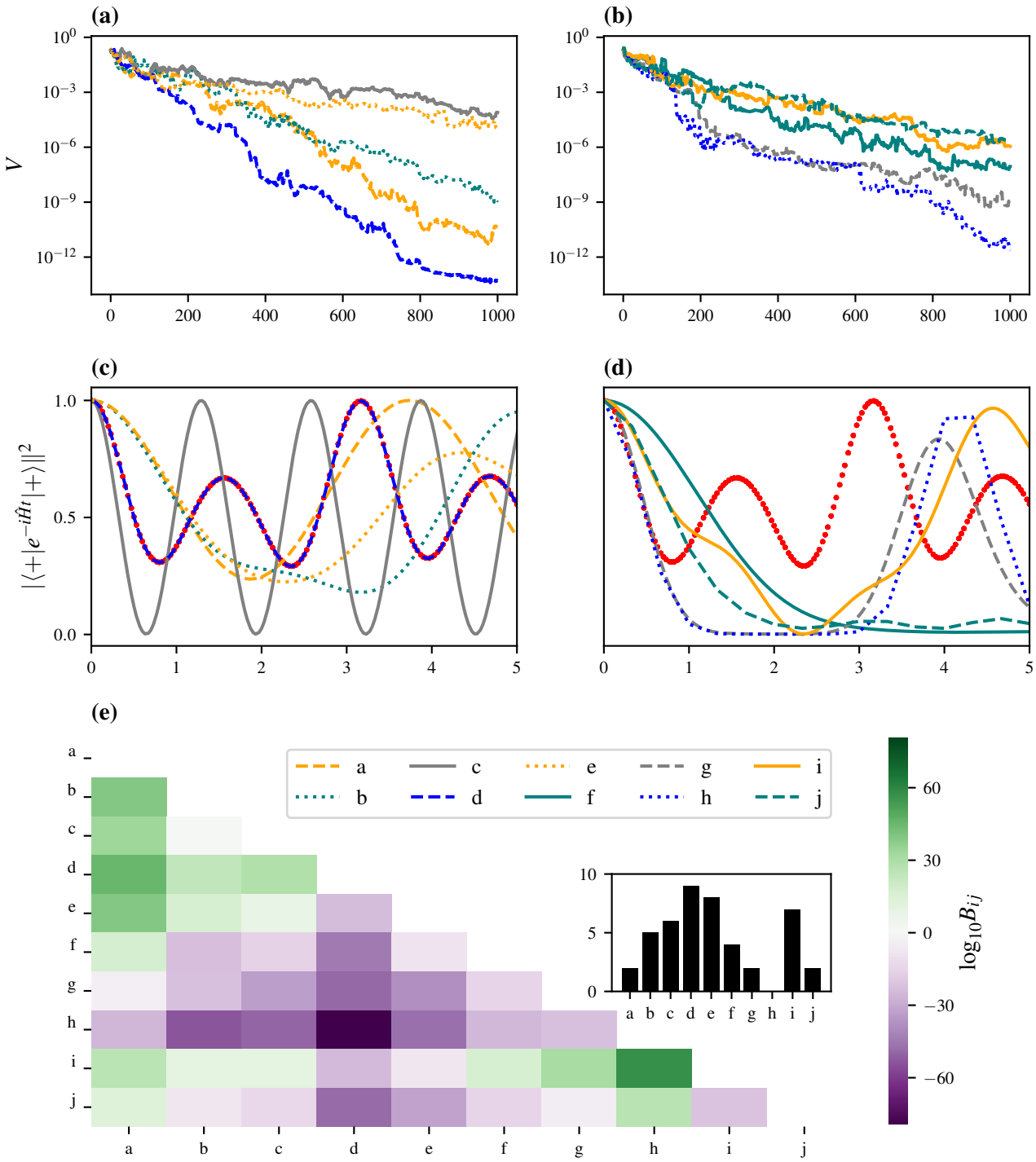

Figure 1.5: QMLA for set of lattices under Ising formalism. The lattice indices correspond to those in Fig. 1.1, and the true system is given by lattice d. (a,b) show the decrease in volume for each model's training phase. (spread over two plots for readibility) (c,d), trained models are used to reproduce dynamics, compared with the dynamics of the true system. (e) Heatmap of $\log_{10} B_{ij}$ between every pair of models. The BF is read as i versus j, where i is the model on the y-axis and j is the model on the x-axis. $\log_{10} B_{ij} > 0$ (green) favours the model listed on the y-axis; $\log_{10} B_{ij} < 0$ (purple) favours the model listed on the x-axis. The inset shows the number of BF comparisons won by each model, i.e. the models' scores.

Algorithm 2: Lattice exploration strategy: consolidation

Input: $\mathbb{H}$ // Set of trained models
Output: $\hat{H}'$ // Favoured model

for $\hat{H}_i \in \mathbb{H}$ **do**
  $s_i \leftarrow 0$ // Score for every model
end
for $\hat{H}_i \in \mathbb{H}$ **do**
  for $\hat{H}_j \in \mathbb{H} \setminus \{\hat{H}_i\}$ **do**
    $B_{ij} \leftarrow BF(\hat{H}_i, \hat{H}_j)$ // Compute Bayes factor via **??**
    if $B_{ij} > 1$ **then**
      $s_i \leftarrow s_i + 1$ // $\hat{H}_i$'s score increases if it is the stronger model
    end
  end
end
$\hat{H}' \leftarrow \arg\max_{s_i} \left(\hat{H}_i\right)$
return $\hat{H}'$

We present the result of these tests in Fig. 1.6, finding in all cases that QMLA identifies $\hat{H}_0$ with success rates at least 70%.

3 The remainder of this thesis is dedicated to cases where we do not prescribe the model set, but instead generate models dynamically.

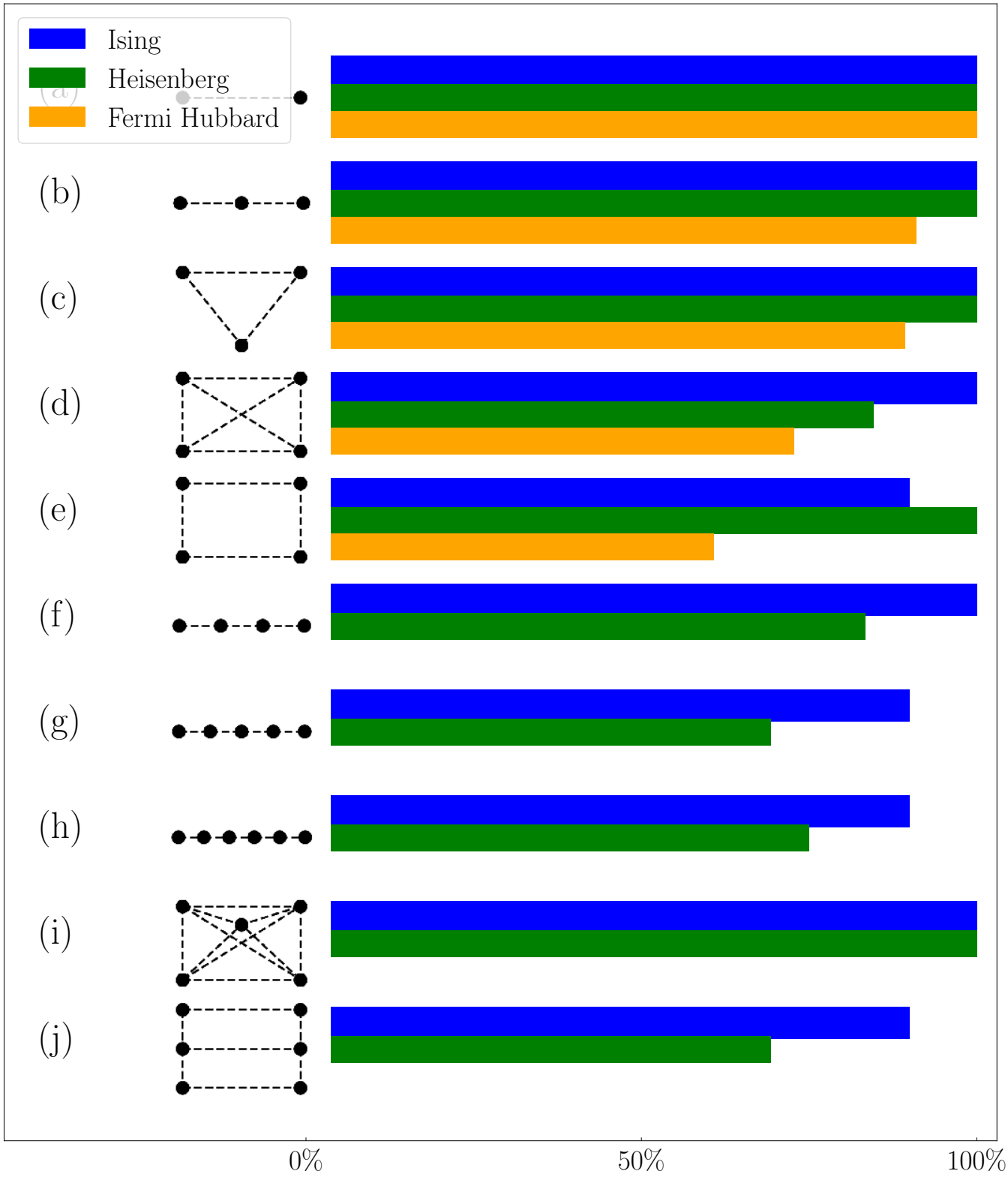

Figure 1.6: Rates of success for QMLA under various conditions. Each lattice is set as the true model $\hat{H}_0$ for ten independent instances. In each instance, the ES considers the available lattices (**a-j** for Ising and Heisenberg cases and **a-e** for the Fermi-Hubbard case), and selects a champion model $\hat{H}'$ as that most consistent with data generated by $\hat{H}_0$.

2

BLACK BOX QUANTUM SYSTEMS

3 GENETIC ALGORITHMS

APPENDIX

A

FIGURE REPRODUCTION

Most of the figures presented in the main text are generated directly by the QMLA framework. Here we list the implementation details of each figure so they may be reproduced by ensuring the configuration in Table A.1 are set in the launch script. The default behaviour of QMLA is to generate a results folder uniquely identified by the date and time the run was launched, e.g. results can be found at the *results directory* qmla/Launch/Jan_01/12_34. Given the large number of plots available, ranging from high-level run perspective down to the training of individual models, we introduce a plot_level $\in \{1, ..., 6\}$ for each run of QMLA: higher plot_level informs QMLA to generate more plots.

Within the results directory, the outcome of the run's instances are stored, with analysis plots broadly grouped as

- evaluation: plots of probes and times used as the evaluation dataset.
- single_instance_plots: outcomes of an individual QMLA instance, grouped by the instance ID. Includes results of training of individual models (in model_training), as well as sub-directories for anlaysis at the branch level (in branches) and comparisons.
- combined_datasets: pandas dataframes containing most of the data used during analysis of the run. Note that data on the individual model/instance level may be discarded so some minor analyses can not be performed offline.
- exploration_strategy_plots plots specifically required by the ES at the run level.
- champion_models: analysis of the models deemed champions by at least one instance in the run, e.g. average parameter estimation for a model which wins multiple instances.
- performance: evaluation of the QMLA run, e.g. the win rate of each model and the number of times each term is found in champion models.
- meta analysis of the algorithm' implementation, e.g. timing of jobs on each process in a cluster; generally users need not be concerned with these.

In order to produce the results presented in this thesis, the configurations listed in Table A.1 were input to the launch script. The launch scripts in the QMLA codebase consist of many configuration settings for running QMLA; only the lines in snippet in Listing A.1 need to be set according to altered to retrieve the corresponding figures. Note that the runtime of QMLA grows quite quickly with N_E, N_P (except for the AnalyticalLikelihood ES), especially for the entire QMLA algorithm; running QHL is feasible on a personal computer in < 30 minutes for $N_e = 1000; N_p = 3000$.

```
#!/bin/bash
```

```
###############
# QMLA run configuration
###############
num_instances=1
run_qhl=1 # perform QHL on known (true) model
run_qhl_mulit_model=0 # perform QHL for defined list of models.
exp=200 # number of experiments
prt=1000 # number of particles

###############
# QMLA settings
###############
plot_level=6
debug_mode=0

###############
# Choose an exploration strategy
###############

exploration_strategy='AnalyticalLikelihood'
```

Listing A.1: "QMLA Launch scipt"

Figure	Exploration Strategy	Algorithm	N_E	N_P	Level	Data	Folder	Name
??	AnalyticalLikelihood	QHL	500	2000	4	Nov_16/14_28	single_instance_plots	learning_summary
Fig. 1.2	DemoIsing	QHL	500	3000	6	Nov_16/23_51	single_instance_plots	learning_summary
Fig. 1.3	DemoIsingFullyParameterised	QHL	1000	3000	6	Nov_16/20_05	single_instance_plots	learning_summary

Table A.1: Implementation details for figures used in the main text.

BIBLIOGRAPHY

[1] Lars Onsager. Crystal statistics. i. a two-dimensional model with an order-disorder transition. *Physical Review*, 65(3-4):117, 1944.

[2] Francisco Barahona. On the computational complexity of ising spin glass models. *Journal of Physics A: Mathematical and General*, 15(10):3241, 1982.

[3] Michael R Garey and David S Johnson. *Computers and intractability*, volume 174. freeman San Francisco, 1979.

[4] Giuseppe E Santoro and Erio Tosatti. Optimization using quantum mechanics: quantum annealing through adiabatic evolution. *Journal of Physics A: Mathematical and General*, 39(36):R393, 2006.

[5] Victor Bapst, Laura Foini, Florent Krzakala, Guilhem Semerjian, and Francesco Zamponi. The quantum adiabatic algorithm applied to random optimization problems: The quantum spin glass perspective. *Physics Reports*, 523(3):127–205, 2013.

[6] Mark W Johnson, Mohammad HS Amin, Suzanne Gildert, Trevor Lanting, Firas Hamze, Neil Dickson, Richard Harris, Andrew J Berkley, Jan Johansson, Paul Bunyk, et al. Quantum annealing with manufactured spins. *Nature*, 473(7346):194–198, 2011.

[7] Walter Greiner, Ludwig Neise, and Horst Stöcker. *Thermodynamics and statistical mechanics*. Springer Science & Business Media, 2012.

[8] John Hubbard. Electron correlations in narrow energy bands. *Proceedings of the Royal Society of London. Series A. Mathematical and Physical Sciences*, 276(1365):238–257, 1963.

[9] Richard T Scalettar. An introduction to the hubbard hamiltonian. *Quantum Materials: Experiments and Theory*, 6, 2016.

[10] Editorial. The hubbard model at half a century. *Nature Physics*, 2013.

[11] Pascual Jordan and Eugene Paul Wigner. über das paulische äquivalenzverbot. In *The Collected Works of Eugene Paul Wigner*, pages 109–129. Springer, 1993.

[12] Mark Steudtner and Stephanie Wehner. Fermion-to-qubit mappings with varying resource requirements for quantum simulation. *New Journal of Physics*, 20(6):063010, 2018.